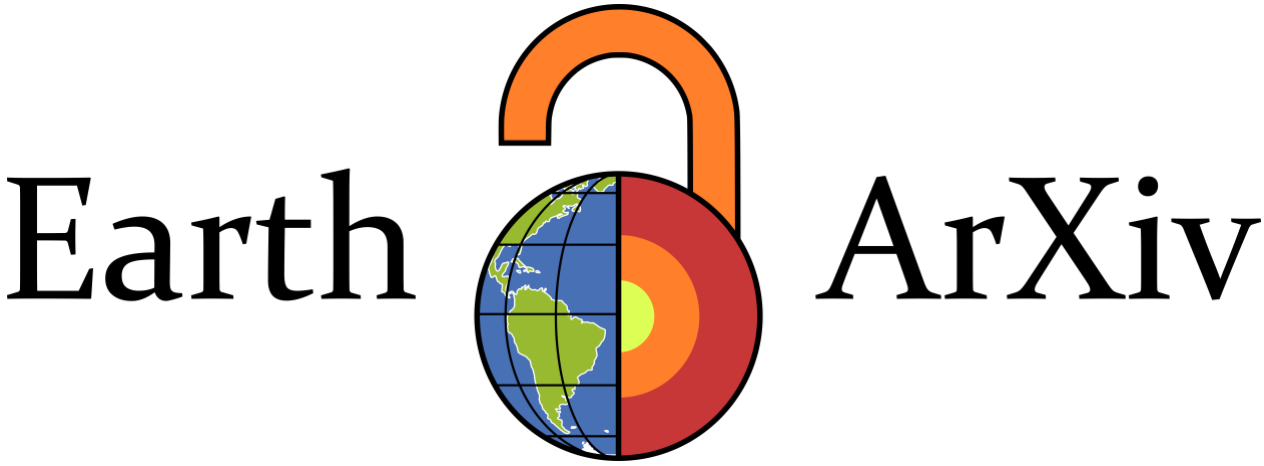

This is a non-peer-reviewed preprint submitted to EarthArXiv.

This manuscript has been submitted for publication in *Science Advances*. Please note the manuscript has yet to be formally accepted for publication. Subsequent versions of this manuscript may have slightly different content. If accepted, the final version of this manuscript will be available via the 'Peer-reviewed Publication DOI' link on the right-hand side of this webpage. Please feel free to contact any of the authors; we welcome feedback.

Manuscript is still under-review by Science Advances
This is a non-peer-reviewed preprint submitted to EarthArXiv

Title: Droughts are dominated by anomalous circulation not anomalous atmospheric moisture content

Authors: SeungUk Kim[1]*, Diego G. Miralles[2], Francina Dominguez[1]*

Affiliations:

[1]Department of Climate, Meteorology, and Atmospheric Sciences, University of Illinois at Urbana-Champaign; Urbana, IL, 61821, United States of America.

[2]Hydro-Climatic Extremes Lab (H-CEL), Ghent University, Ghent, 9000, Belgium.

*Corresponding author. Email: seunguk2@illinois.edu; francina@illinois.edu

Abstract: Agricultural drought is a sustained soil moisture deficit caused by reduced net moisture flux to the land surface. We show that agricultural droughts can occur when the atmosphere is anomalously wet, challenging the assumption that surface drying reflects atmospheric moisture deficits. Precipitation declines during drought even under increased atmospheric moisture, indicating low precipitation efficiency: subsidence and reduced relative humidity suppress condensation, while enhanced moisture divergence exports water from the column. Moisture budget analysis reveals that divergence driven by anomalous circulation accounts for most of the drying, while advection by anomalous winds governs the spatial pattern of total column water. In contrast, advection of anomalous moisture largely counteracts drying. Droughts are thus dominated by anomalous winds that export water, rather than by limited moisture supply.

Preprint

Main Text: Agricultural drought refers to sustained soil moisture deficits resulting from prolonged reductions in net freshwater influx from the atmosphere to the land surface (1), quantified as precipitation minus evaporation ($P - E$). Compared with other natural disasters, droughts are characterized by longer duration and broader spatial extent, which make their impacts especially pervasive and costly (2–6). Persistent droughts cause substantial damage to ecosystems and agriculture, including crop failure, thereby reducing food production and imposing major economic losses (4, 7–12). Further, drought risks are projected to increase in many regions, with droughts becoming more frequent, severe, and persistent under higher warming scenarios (1, 11–17).

While agricultural drought is defined by reduced soil moisture, it can also be viewed from an atmospheric perspective. Deficits in $P - E$ arise from imbalances in the atmospheric moisture budget, as described by the atmospheric moisture budget equation,

$$P - E = -\frac{\partial \langle q \rangle}{\partial t} - \nabla \cdot \langle q\vec{u} \rangle \quad (1)$$

where q is specific humidity, $\vec{u}$ is horizontal wind, and $\langle A \rangle = \frac{1}{g\rho_w}\int_0^{p_s} A dp$ (18–20). Here, g is gravitational acceleration, ρ_w is density of liquid water, and p_s is surface pressure, and A is any atmospheric variable. In Eq. 1, $P - E$ represents the atmospheric net sink and source of moisture, balanced by changes in atmospheric moisture storage and by moisture convergence.

Prior work has linked drought to different physical drivers. Reduced moisture supply and transport, together with the downwind propagation of drought from upwind evaporation deficits through land-atmosphere interactions (21, 22), has been studied largely with Lagrangian moisture tracking (22–25); large-scale circulation (26, 27), dry advection (24, 28), subsidence, and low-level divergence (19, 20) have been diagnosed within Eulerian moisture budgets (18–20, 27–31). These physical drivers, however, have typically been examined in isolation or applied to individual regions, leaving their relative contributions to any given drought—and whether the same balance of mechanisms holds across different climates—unresolved.

The Eulerian moisture budget is well suited to close this gap, because it partitions the $P - E$ deficit into all of these contributions simultaneously: the roles of specific humidity (thermodynamic) and circulation (dynamic), and of advection and divergence, within a single consistent framework (18–20). Here we apply this decomposition across eleven regions in both hemispheres to show that atmospheric moisture deficits play only a secondary role in drought, while anomalous circulation dominates. We first show how moisture-flux divergence balances the $P - E$ budget in ERA5 reanalysis (32, 33) over 1979–2022. We then show that anomalies in circulation, rather than in moisture, drive the drying during drought months, identified from normalized ERA5 surface soil moisture anomalies, with the Standardized Precipitation-Evapotranspiration Index (SPEI) (34) used as a consistency check. Finally, we decompose the $P - E$ budget to quantify the relative contributions of anomalous circulation, anomalous humidity, their covariance, and the divergence and advection terms (18–20) for droughts across these regions using reanalysis data (35).

Moisture Convergence explains Global $P - E$

At monthly or longer timescales, the net horizontal export of moisture from the air column, or the divergence of vertically integrated moisture fluxes ($\langle q\vec{u} \rangle$; WVDIV), approximately balances $P - E$, as implied by Eq. 1. This balance is reflected in the climatological monthly $P - E$ cycles during April–September, the Northern Hemisphere warm season, when soil moisture impacts on

agriculture are critical (Fig. 1, top). Similar results are found for October–March, the warm season in the Southern Hemisphere (Fig. 1, bottom). Monthly time series of $P - E$ and WVDIV are strongly correlated over most of the globe, with a global land average correlation of -0.80 (see fig. S1). Exceptions are found in very arid regions such as the Sahara, where both P and E are small and nearly equal, and $P - E$ approaches zero. Conversely, $P - E$ is not significantly correlated with the total amount of water in the air column or the moisture storage tendency (fig. S1). Climatological P shows higher correlation with WVDIV than atmospheric moisture or its tendency (fig. S1). Thus, climatological $P - E$ bears little resemblance to the total amount of moisture in the atmosphere or its tendency, which is small at these scales. Instead, the convergence/divergence of atmospheric moisture dictates the spatial patterns of $P - E$.

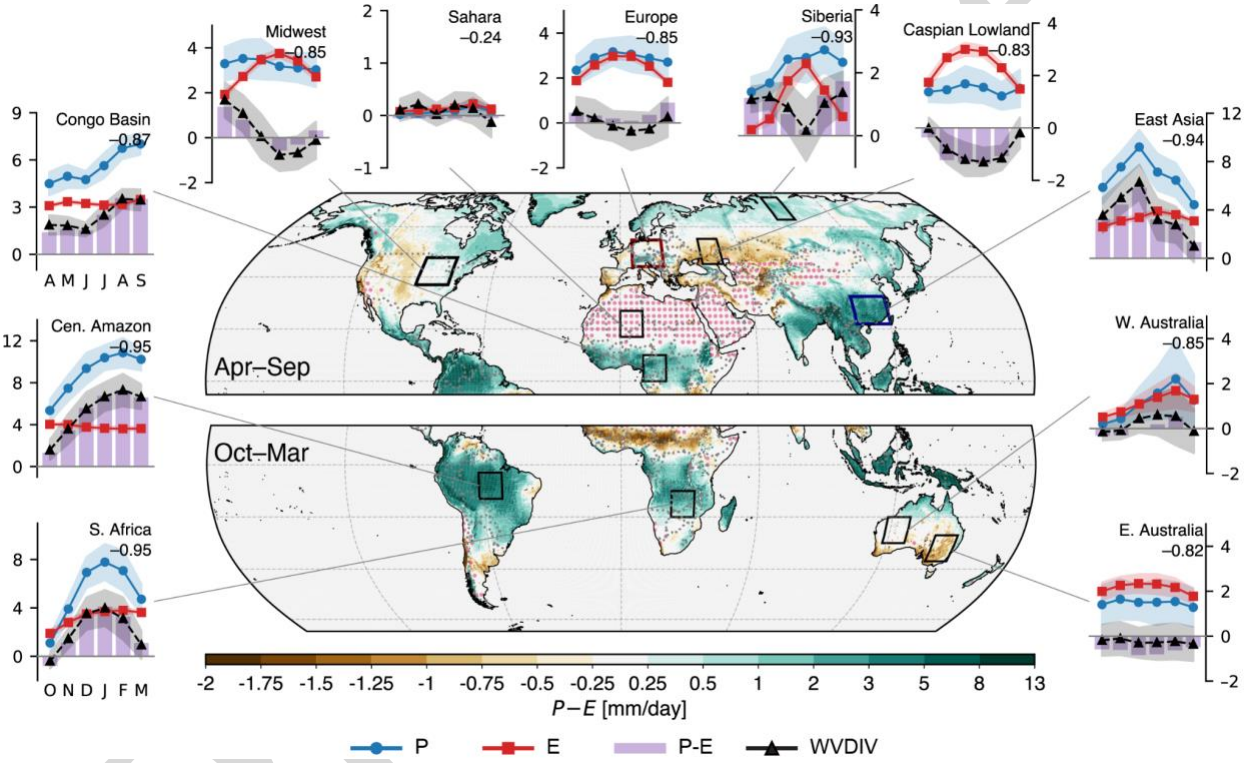

Fig. 1. Climatological surface moisture fluxes and divergence of atmospheric moisture fluxes from warm season 1979–2022. The global map shows warm season $P - E$ climatology (shading) for April to September in the Northern Hemisphere (75°N to 5°S) and October to March in the Southern Hemisphere (15°N to 65°S). Pink stippling denotes regions of low correlation of $P - E$ and divergence of vertically integrated moisture fluxes (WVDIV) ($r < 0.5$). Subplots of selected regions show monthly climatology of P (blue), E (red), $P - E$ (purple columns), and WVDIV (black) converted to mm/day with correlation coefficient between $P - E$ and WVDIV. Shadings in subplots denote ± 1 standard deviation.

Regions of strong low-level convergent moisture fluxes, including those within the Intertropical Convergence Zone and monsoon regions such as East Asia and India, have high precipitation, strong evaporation, and positive $P - E$. In the midlatitudes of North America and Eurasia, both P and E are generally lower and $P - E$ is smaller in magnitude than in the Tropics. In humid regions where P variability is the primary control on $P - E$, such as East Asia and the northern Amazon (Fig. 1), P covaries with WVDIV (fig. S1).

Droughts caused by suppressed precipitation efficiency

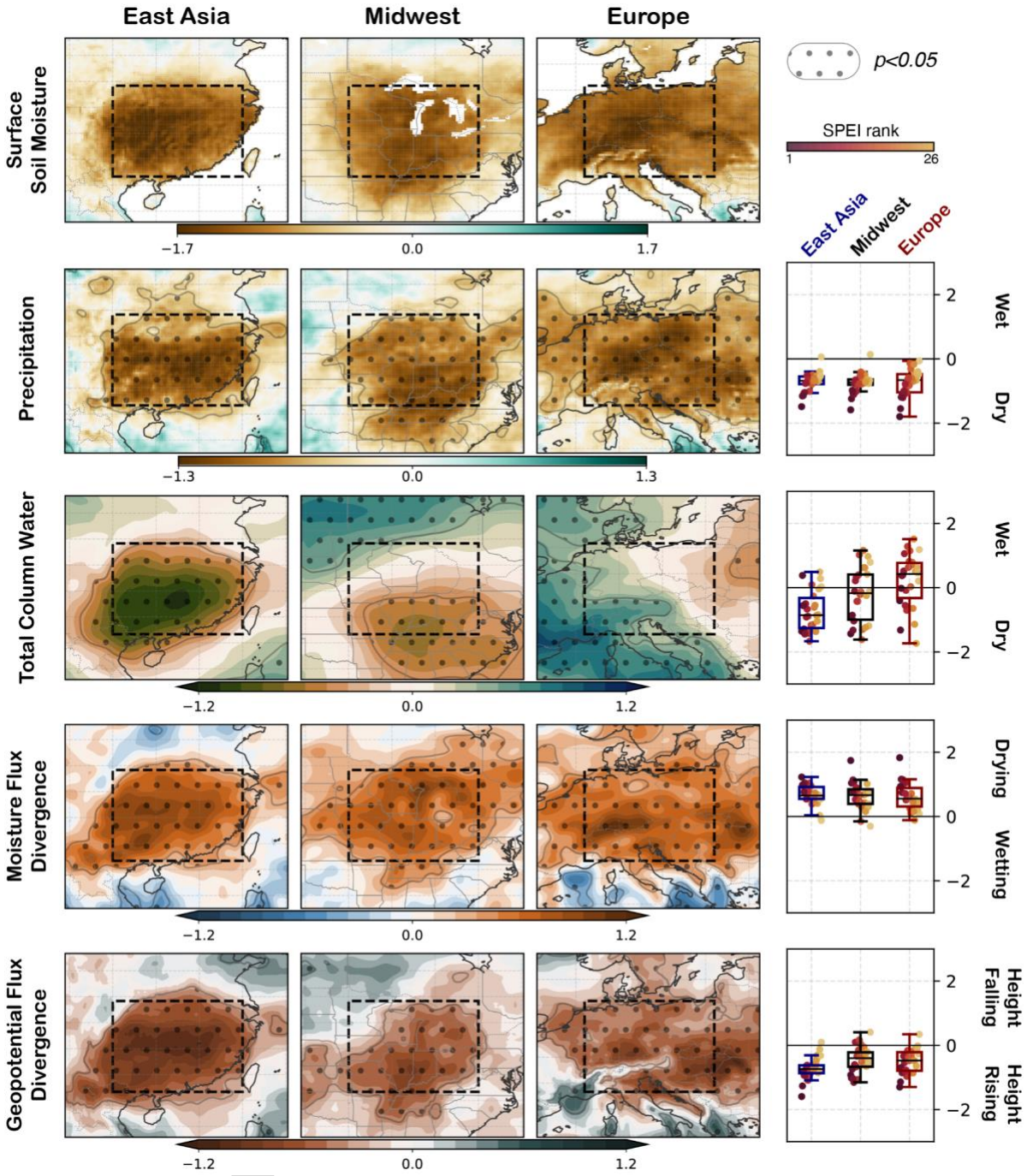

Fig. 2. Composite maps and normalized anomalies during the driest months. Mean surface soil moisture, precipitation, total column water, divergent moisture flux, and divergent geopotential flux averaged over the driest 10% months, a total of 26 months during April–September from 1979 to 2022. Regions where values differ significantly from zero ($p < 0.05$) are outlined and stippled. Dots in bar plots show normalized monthly anomalies for each domain, which is bounded by dashed box, colored by the rank of each domain's SPEI. All units are dimensionless.

We analyze the 10% driest months during the 1979–2022 warm season, identified using domain-averaged normalized surface soil moisture anomalies for three selected regions: East Asia, the

Midwestern US and Europe (Fig. 2, top row). Analysis of eight additional regions in the Northern and Southern Hemispheres is shown in the Supplementary Material. While the three selected regions exhibit coherent dry surface conditions, these spatial patterns are not robustly consistent with the normalized total column water (TCW) anomalies (Fig. 2, third row). In East Asia, the atmospheric column was generally dry, broadly consistent with the surface drought index. Most dry events were accompanied by below-normal atmospheric water (median -0.85), although several events occurred during above-normal atmospheric water conditions, including the July 2013 drought (36) with a positive precipitable water anomaly ($+0.49$).

In the Midwestern US, dry-surface wet-atmosphere conditions are not uncommon. Although much of the region exhibits reduced atmospheric moisture during the driest months, the northwestern region shows positive TCW anomalies coincident with significant dry soil moisture conditions. Consistently, while median normalized TCW during drought was -0.17, several events have positive domain-averaged TCW anomalies, indicating that in the Midwest drought can coexist with anomalously moist atmospheric conditions. One such case was July 2012, one of the most severe droughts in the Midwest, when the TCW anomaly reached $+1.02$. Yet, previous studies attributed the associated $P - E$ deficit during this event to dry advection (21, 22, 28).

The most counterintuitive signal emerges in Europe, where the southwestern half of the domain exhibits significantly positive TCW anomalies. In other words, the most extreme dry surface conditions in Europe are most often accompanied by an anomalous wet atmospheric column. The median TCW anomaly is $+0.43$. Notably, the 2003, 2018, and 2022 European droughts – all among the most severe reported in the region (37–40) – show TCW anomalies of $+1.05$, $+1.28$, and $+1.51$ respectively.

These results indicate that extreme surface drought is not necessarily associated with reduced atmospheric moisture content. The same conclusion holds for events with even drier surface conditions (driest 5% months; fig. S2). Thus, tracing the origin of reduced moisture transport alone cannot fully explain drought dynamics, because moistening of the atmospheric column may still occur while dry surface conditions persist. For example, increased atmospheric moisture demand during droughts can enhance evaporation where surface water remains available, adding moisture to the atmospheric column even as surface drying continues (41–43), as reflected by varied spatial patterns of anomalous E (fig. S3). We can see this in the northern Midwest, where evaporation (fig. S3) and atmospheric moisture content (Fig. 2) is higher during drought periods. Analysis of E also reveals that the spatial pattern of $P - E$ anomalies is significantly different from those of E anomalies, indicating the more dominant role of P.

We see that drought months are characterized by significant negative precipitation anomalies, as shown using the normalized precipitation anomalies (Fig 2, second row) and Standardized Precipitation Index (SPI) (fig. S4), indicating that, even when precipitable water is sufficiently available, precipitation is suppressed. Defining precipitation efficiency as the ratio of P to TCW, our analysis reveals a decrease in precipitation efficiency during drought periods that we can attribute to both local thermodynamics and large-scale circulation. Locally, decreased soil moisture will generally tend to increase sensible heat flux in areas of decreased E, leading to higher temperature and exponentially higher saturation vapor pressure in the region. We see this in the sharp decrease of relative humidity (RH) in all regions during the driest months (fig. S5). Sharply reduced RH will decrease condensation and local P.

Preprint

Changes in $P - E$ can also be examined in terms of changes in atmospheric circulation as reflected in WVDIV, which represents the net horizontal export of moisture, and shows spatial patterns closely aligned with those of the drought index across all regions (Fig. 2, fourth row). Unlike TCW, the composite of WVDIV exhibits consistently positive anomalies, indicating enhanced divergence of moisture flux, or greater export of moisture from the region during droughts. Enhanced divergence is also present during droughts with positive TCW anomalies. In addition, the most severe drought events (Fig. 2, bar plot dark dots) tend to have the largest positive WVDIV anomalies (fig. S6). Because atmospheric moisture is concentrated near the surface (fig. S7), WVDIV is particularly sensitive to low-level circulation and emphasizes enhanced outflow of moisture in the lower levels of the atmosphere.

Circulation in the upper-atmosphere, despite containing no direct information about moisture, also helps explain surface drying. The negative anomalies of the vertically integrated geopotential flux ($\nabla \cdot \int_0^{p_s} \Phi \vec{u} dp$; VIGD), show spatial patterns that are closely aligned with surface soil moisture (Fig. 2, bottom row). Negative VIGD anomalies indicate enhanced convergence of geopotential flux, leading to the development of high-pressure systems. Because geopotential increases with height (fig. S7), VIGD is more strongly influenced by upper-level winds and highlights enhanced convergent flow aloft. Thus, extreme surface drought is robustly associated with enhanced low-level moisture outflow, and enhanced upper-level high-pressure system development (9, 30, 44, 45). High pressure aloft suppresses precipitation development due to large-scale subsidence which inhibits ascent of moist air masses, combined with adiabatic heating that further increases local temperature and decreases relative humidity, as discussed above.

The results presented above are consistent when we repeat the analysis using selected drought events based on the Standardized Precipitation-Evapotranspiration Index (SPEI) instead of soil moisture anomalies (figs. S8–9). The strong correlation between SPEI, WVDIV and VIGD, but much weaker relationship between SPEI and TCW, particularly in Europe, suggests that atmospheric and soil moisture drought are driven by robust dynamical mechanisms rather than atmospheric moisture constraints alone (Fig. 2, right scatterplot, and fig. S6).

When analyzing all eleven different regions throughout the globe we find that this behavior is also observed during their respective warm seasons, except in a few water-limited regions (figs. S10–S12). This indicates that the results are globally generalizable, except in regions with very low P and E. Together, these results indicate that $P - E$ is driven by P deficits. Critically, P deficits can occur despite enhanced moisture in the atmospheric column, indicating reduced precipitation efficiency. Reduced P efficiency is partly a result of sharp decreases in relative humidity due to higher temperature and subsidence-induced adiabatic heating from above. Large-scale subsidence also reduces precipitation efficiency by inhibiting ascent of air masses. The fact that geopotential flux convergence, a variable that contains no direct information about atmospheric moisture, better explains drought spatial variability than column precipitable water suggests that atmospheric circulation plays a fundamental role in drought dynamics.

Decomposing the $P - E$ deficit

To understand the dominant factors that cause changes in atmospheric circulation, as reflected in WVDIV, we use the moisture budget decomposition of anomalous moisture-flux divergence, $\nabla \cdot (qu)'$. In the analysis below, the anomalies (as denoted by $'$) represent the departures from climatology during periods of drought. Since the moisture flux depends on both moisture ($\bar{q} + q'$) and winds ($\bar{u} + u'$), the anomalous moisture flux $(qu)'$ can be decomposed

Preprint

into three contributions: anomalous circulation acting on climatological moisture ($\bar{q}u'$), anomalous moisture transported by climatological circulation ($q'\bar{u}$), and their covariance ($q'u'$). We refer to these as the dynamic, thermodynamic, and covariance terms, respectively. Moisture flux divergence can be further decomposed into components associated with divergent flow ($q\nabla \cdot u$) and advection associated with moisture-gradients ($u \cdot \nabla q$), yielding six terms in total:

$$\nabla \cdot (qu)' = \bar{q}\nabla \cdot u' + q'\nabla \cdot \bar{u} + (q'\nabla \cdot u' - \overline{q'\nabla \cdot u'})$$
$$+u' \cdot \nabla\bar{q} + \bar{u} \cdot \nabla q' + (u' \cdot \nabla q' - \overline{u' \cdot \nabla q'}) \quad (2)$$

Here, the first line shows anomalous divergence terms, and the second line shows anomalous advection terms. In each line, the first term denotes the dynamic component, the second term denotes the thermodynamic component, and the third term denotes the covariance component.

The full mathematical decomposition is provided in Materials and Methods. We quantify all six terms and compare them with changes in $P - E$. For example, if drought conditions are primarily driven by mass divergence associated with anomalous circulation, the dynamic divergence term ($\bar{q}\nabla \cdot u'$) should dominate. All six terms in the Midwestern US are discussed here, and a sum of the six decomposed terms (figs. S13–14) are shown in supplementary, along with other regions (figs. S15–20). Region-averaged values of each term during drought months are summarized in tables S1 and S2.

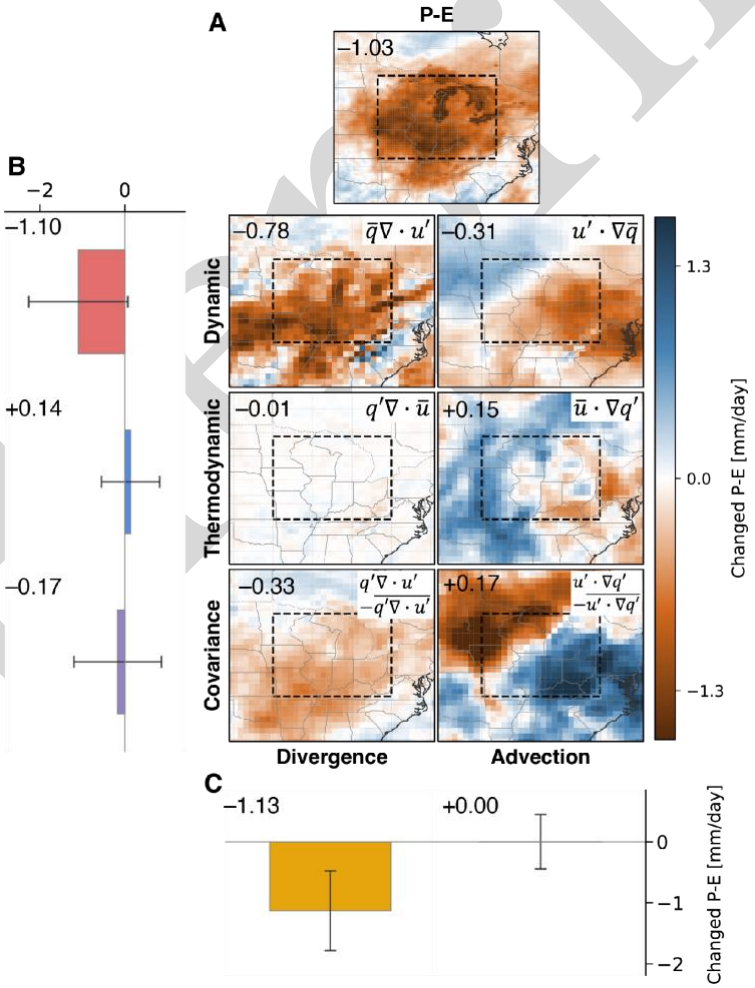

Fig. 3. $P - E$ anomalies and decomposition of anomalous moisture budget terms during drought months in the Midwestern US. (A) Mean anomalous terms derived from 3-hourly

Preprint

ERA5 data, for the top 10% driest months are shown in mm/day relative to the 1981–2020 monthly climatology. The 1981–2020 climatology differs from the baseline used in previous figures. Each panel shows the mathematical expression for the corresponding term and region-averaged values over the dashed contour. The sum of the six decomposed terms in panel A equals the anomalous vertically integrated moisture divergence term, and the residual difference between this sum and the $P - E$ anomaly represents the surface term. (B and C) Bar plots show the sums of the region-averaged terms for each row (B) and column (C). Error bars in each bar plot indicate ± 1 standard deviation range.

Circulation anomalies dominate $P - E$ deficit

Analyzing the composite of the six WVDIV terms for the driest 10% drought months in the Midwestern US, we find the average decrease in local $P - E$ (-1.03 mm/day) is dominated by the contribution from anomalous circulation (u') (-1.10 mm/day; Fig. 3B pink bar), particularly through the divergence term ($\bar{q}\nabla \cdot u'$), which is strongly negative over much of the domain. This term (Fig. 3B first row left) most closely reproduces the observed $P - E$ pattern (Fig. 3A top), including pronounced drying over the western Midwestern US and strong anomalies near the Great Lakes. Its magnitude (-0.78 mm/day) is also comparable to the total $P - E$ deficit, indicating that divergence of moisture driven by anomalous circulation alone accounts for most of the drying. The dominance of the dynamic contribution of the divergence term is also found in Europe, East Asia, and other regions around the globe (figs. S15–22).

Circulation anomalies also contribute to drying through the advection term ($u' \cdot \nabla\bar{q}$) (Fig. 3B first row right), although its contribution is smaller (-0.31 mm/day) than the divergence term. This term produces drying over most of the domain but wetting in the northwestern part of the region, closely resembling the anomalous TCW pattern (Fig. 2). Interestingly, a similar correspondence appears over East Asia, Europe, and other regions, where the dynamic component of the advection term resembles the normalized TCW anomaly patterns: broad drying in East Asia and a wet anomaly over western Europe (figs. S15 to S18). This suggests that advection by anomalous winds controls the redistribution of atmospheric moisture during extreme droughts, thereby modulating the anomalous spatial pattern of precipitable water.

Moisture anomalies and covariance offset wind-change effects

In contrast to the circulation anomalies, the moisture-anomaly contribution (q') ($+0.14$ mm/day; Fig. 3B blue bar) significantly contributes to increasing $P - E$, thereby offsetting the drying driven by circulation changes, especially through the advection term (Fig. 3B second row right, $\bar{u} \cdot \nabla q'$). The strongest wetting signal appears where the largest $P - E$ deficits occur, particularly over the western half of the domain, indicating that advection of anomalous moist air counteracts the drying. By comparison, the divergence term associated with moisture anomalies (Fig. 3B second row left) is weak (-0.01 mm/day) and mostly insignificant. A similar structure is found in most of the other regions around the globe, where the thermodynamic contribution appears mainly in the advection term with a wetting signal, and only weak signals in the divergence term.

The covariance contribution ($q'u'$) (-0.17 mm/day; Fig. 3B purple bar), which reflects the combined effect of circulation and moisture anomalies, is also larger in the advection term than in the divergence term (Fig. 3B bottom). In the Midwest, this term produces strong drying in the northwest, where TCW indicates anomalous wet atmospheric condition, helping explain the local $P - E$ deficit that is not fully captured by the circulation-anomaly contribution alone. Over most of the domain, however, the covariance term shows wetting that offsets the drying associated with the dynamic contribution to advection (Fig. 3B first row right). Thus, within the advection

Preprint

term, the signals produced by circulation anomalies are substantially reduced once concurrent moisture anomalies are considered. As a result of these compensating effects, the total advection term is zero (Fig. 3C blue bar) while the divergence term dominates (−1.13 mm/day; Fig. 3C yellow bar). The covariance contribution to the divergence term, on the other hand, is weak but shows generalized drying (−0.33 mm/day), with a similar spatial pattern to that of the circulation-anomaly contribution.

A similar overall structure is also found in other regions (figs. S15 to S20). In East Asia, the covariance contribution of the advection term generally produces wetting across the domain, whereas in Europe it produces drying in the west and wetting in the east. In both regions, these patterns are broadly opposite to the TCW anomalies. The associated divergence terms are again weak and generally have drying patterns.

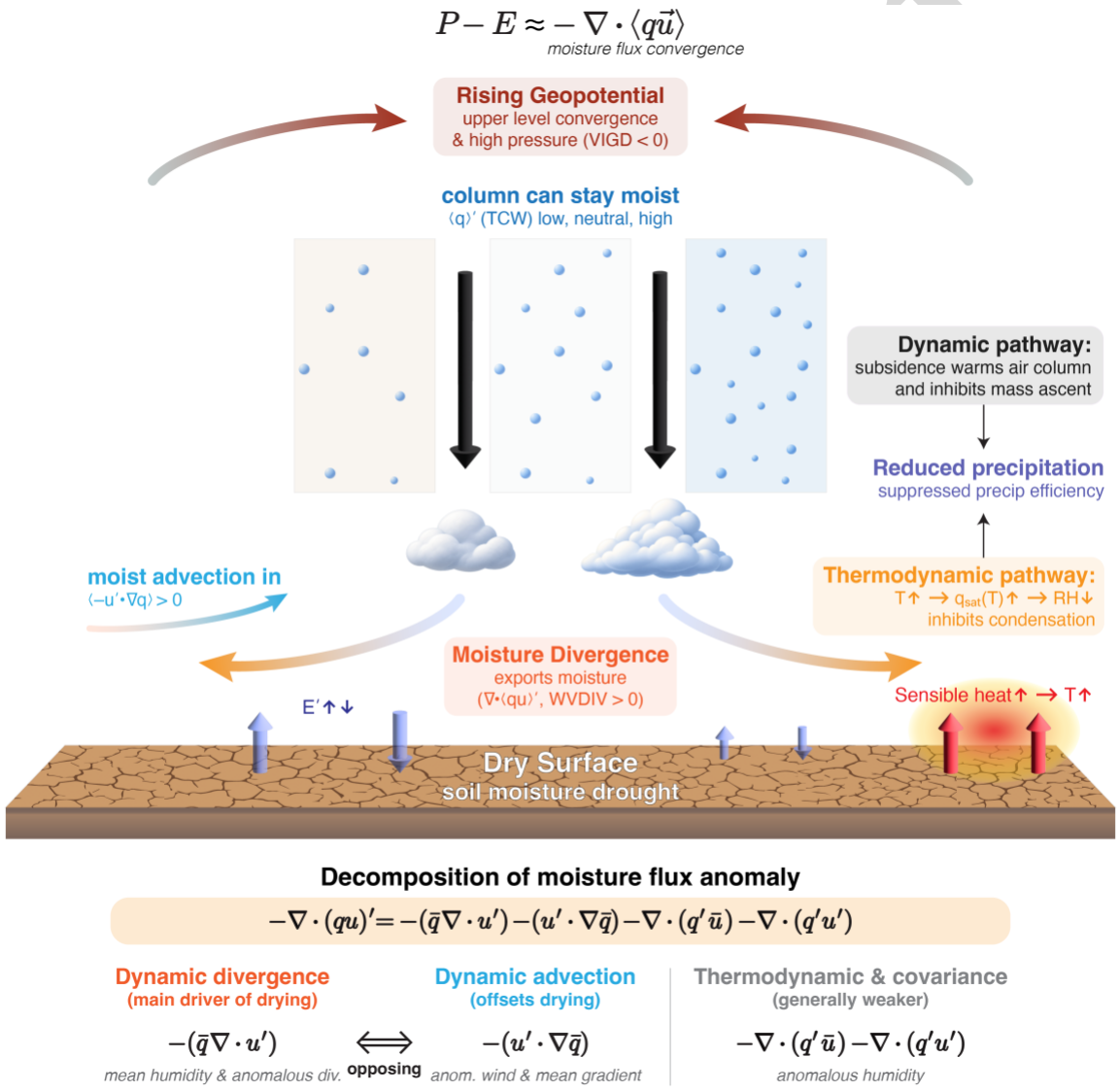

Fig. 4. Conceptual diagram of drought dynamics. Key components of drought dynamics and their roles in surface drying are illustrated. Shading highlights processes associated with land surface drying, including rising geopotential and enhanced moisture divergence, which reduce precipitation through dynamical and thermodynamical pathways by exporting moisture and inhibiting condensation, respectively. Key terms in the moisture flux divergence are also shown,

highlighting contributions of dynamic divergence and advection that drive and oppose drying, respectively.

Implications

Our findings suggest that dry surface conditions are not necessarily associated with dry atmospheric conditions; rather, $P - E$ deficits are consistently associated with reduced P efficiency linked to local near surface thermodynamics and circulation anomalies that dominate the $P - E$ budget (Fig. 4). Across several regions of the globe, droughts occurred under neutral or even positive total column water anomalies, whereas circulation-related indicators showed a coherent drying signal at the monthly timescale. Enhanced low-level divergent flow and rising geopotential heights aloft are robust indicators of drought that can lead to a sharp decrease in P efficiency. These results support earlier work showing that droughts are affected by large-scale circulation anomalies (27, 30, 44, 45), including those linked to remote sea surface conditions (26, 27, 45), and associated low-level divergence (20).

The Eulerian approach applied here directly quantifies the physical processes contributing to local surface drying. Moisture budget analysis of $P - E$ reveals that anomalous circulation drives surface drying and promotes moisture redistribution, while anomalous moisture and circulation-moisture covariance partly offset that drying through advection. The consistency of this result across regions with contrasting moisture anomalies during droughts suggests that circulation-based diagnostics may improve our global mechanistic understanding of drought and its propagation (46), for which the governing processes remain incompletely understood (41). In particular, large-scale circulation anomalies induced by soil moisture anomalies (47, 48) may provide one pathway linking existing drought conditions to subsequent drying elsewhere.

References and Notes

1. S. I. Seneviratne, X. Zhang, M. Adnan, W. Badi, C. Dereczynski, A. Di Luca, S. Ghosh, I. Iskander, J. Kossin, S. Lewis, F. Otto, I. Pinto, M. Satoh, S. M. Vicente-Serrano, M. Wehner, B. Zhou, "Chapter 11: Weather and Climate Extreme Events in a Changing Climate" in *Climate Change 2021: The Physical Science Basis*, V. Masson-Delmotte, P. Zhai, A. Pirani, S. L. Connors, C. Péan, S. Berger, N. Caud, Y. Chen, L. Goldfarb, M. I. Gomis, M. Huang, K. Leitzell, E. Lonnoy, J. B. R. Matthews, T. K. Maycock, T. Waterfield, K. Yelekçi, R. Yu, B. Zhu, Eds. (Intergovernmental Panel on Climate Change, 2021); https://www.ipcc.ch/report/ar6/wg1/chapter/chapter-11/.
2. National Research Council, "Chapter 2: Drought" in *Understanding Multiple Environmental Stresses* (National Academies Press, Washington, DC, 2007), pp. 15–26.
3. D. A. Wilhite, "Chapter 1: Drought as a Natural Hazard: Concepts and Definitions" in *Drought: A Global Assessment*, D. A. Wilhite, Ed. (Routledge, London, 2000), pp. 3–18.
4. NOAA National Centers for Environmental Information, *U.S. Billion-Dollar Weather and Climate Disasters* (2025); doi:10.25921/stkw-7w73.
5. W. R. L. Anderegg, C. Schwalm, F. Biondi, J. J. Camarero, G. Koch, M. Litvak, K. Ogle, J. D. Shaw, E. Shevliakova, A. P. Williams, A. Wolf, E. Ziaco, S. Pacala, Forest ecology. Pervasive drought legacies in forest ecosystems and their implications for carbon cycle models. *Science* **349**, 528–532 (2015).
6. T. D. Huynh, T. H. Nguyen, C. Truong, Climate risk: The price of drought. *J. Corp. Finance* **65**, 101750 (2020).

Preprint

7. C. Lesk, P. Rowhani, N. Ramankutty, Influence of extreme weather disasters on global crop production. *Nature* **529**, 84–87 (2016).
8. G. Leng, J. Hall, Crop yield sensitivity of global major agricultural countries to droughts and the projected changes in the future. *Sci. Total Environ.* **654**, 811–821 (2019).
9. M. L. Goulden, R. C. Bales, California forest die-off linked to multi-year deep soil drying in 2012–2015 drought. *Nat. Geosci.* **12**, 632–637 (2019).
10. A. I. J. M. van Dijk, H. E. Beck, R. S. Crosbie, R. A. M. de Jeu, Y. Y. Liu, G. M. Podger, B. Timbal, N. R. Viney, The Millennium Drought in southeast Australia (2001–2009): Natural and human causes and implications for water resources, ecosystems, economy, and society. *Water Resour. Res.* **49**, 1040–1057 (2013).
11. S. M. Vicente-Serrano, S. M. Quiring, M. Peña-Gallardo, S. Yuan, F. Domínguez-Castro, A review of environmental droughts: Increased risk under global warming? *Earth-Sci. Rev.* **201**, 102953 (2020).
12. M. A. Caretta, A. Mukherji, M. Arfanuzzaman, R. A. Betts, A. Gelfan, Y. Hirabayashi, T. K. Lissner, J. Liu, E. Lopez Gunn, R. Morgan, S. Mwanga, S. Supratid, Chapter 4: Water, in *Climate Change 2022: Impacts, Adaptation and Vulnerability. Contribution of Working Group II to the Sixth Assessment Report of the Intergovernmental Panel on Climate Change*, H.-O. Pörtner, D. C. Roberts, M. Tignor, E. S. Poloczanska, K. Mintenbeck, A. Alegría, M. Craig, S. Langsdorf, S. Löschke, V. Möller, A. Okem, B. Rama, Eds. (Cambridge Univ. Press, 2022), pp. 551–712.
13. S. H. Gebrechorkos, et al., Warming accelerates global drought severity. *Nature* (2025).
14. J. I. Christian, J. B. Basara, E. D. Hunt, J. A. Otkin, J. C. Furtado, X. Xiao, Global projections of flash drought show increased risk in a warming climate. *Commun. Earth Environ.* **4** (2023).
15. A. Berg, K. Findell, B. Lintner, A. Giannini, S. I. Seneviratne, B. van den Hurk, R. Lorenz, A. Pitman, S. Hagemann, A. Meier, F. Cheruy, A. Ducharne, S. Malyshev, P. C. D. Milly, Land–atmosphere feedbacks amplify aridity increase over land under global warming. *Nat. Clim. Change* **6**, 869–874 (2016).
16. P. B. Duffy, P. Brando, G. P. Asner, C. B. Field, Projections of future meteorological drought and wet periods in the Amazon. *Proc. Natl. Acad. Sci. U.S.A.* **112**, 13172–13177 (2015).
17. A. P. Williams, E. R. Cook, J. E. Smerdon, B. I. Cook, J. T. Abatzoglou, K. Bolles, S. H. Baek, A. M. Badger, B. Livneh, Large contribution from anthropogenic warming to an emerging North American megadrought. *Science* **368**, 314–318 (2020).
18. R. Seager, N. Henderson, Diagnostic computation of moisture budgets in the ERA-Interim reanalysis with reference to analysis of CMIP-archived atmospheric model data. *J. Clim.* **26**, 7876–7901 (2013).
19. R. Seager, D. Neelin, I. Simpson, H. Liu, N. Henderson, T. Shaw, Y. Kushnir, M. Ting, B. Cook, Dynamical and thermodynamical causes of large-scale changes in the hydrological cycle over North America in response to global warming. *J. Clim.* **27**, 7921–7948 (2014).
20. B. Jong, M. Newmann, A. Hoell, Subseasonal Meteorological Drought Development over the Central United States during Spring (2022). doi:10.1175/JCLI-D-21-0435.1
21. D. L. Schumacher, J. Keune, P. Dirmeyer, et al., Drought self-propagation in drylands due to land–atmosphere feedbacks. *Nat. Geosci.* **15**, 262–268 (2022).
22. J. E. Herrera-Estrada, J. A. Martinez, F. Dominguez, K. L. Findell, J. Sheffield, E. F. Wood, Reduced moisture transport linked to drought propagation across North America. *Geophys. Res. Lett.* **46**, 5243–5253 (2019).
23. L. Gimeno-Sotelo, et al., Unravelling the origin of the atmospheric moisture deficit in droughts. *npj Clim. Atmos. Sci.* **7**, art. 18 (2024).

Preprint

24. J. Eiras-Barca, et al., Revisiting the Impact of Moisture Transport Deficit on Droughts. *WIREs Clim. Change* (2025).
25. A. Drumond, M. Stojanovic, R. Nieto, S. M. Vicente-Serrano, L. Gimeno, Linking anomalous moisture transport and drought episodes in the IPCC reference regions. *Bull. Am. Meteorol. Soc.* **100**, 1481–1498 (2019).
26. J. Namias, Some meteorological aspects of drought with special references to the summers of 1952-54 over the United States, *Mon. Weather Rev*. **83**, 199–205 (1955).
27. K. E. Trenberth, G. W. Branstator, P. A. Arkin, Origins of the 1988 North American drought. *Science* **242**, 1640–1645 (1988).
28. A. Erfanian, R. Fu, The role of spring dry zonal advection in summer drought onset over the US Great Plains. *Atmos. Chem. Phys*. **19**, 15199–15216 (2019).
29. Y. Zhuang, R. Fu, B. D. Santer, R. E. Dickinson, A. Hall, Dryness over the U.S. Southwest, a springboard for cold season Pacific SST to influence summer drought over the U.S. Great Plains. *J. Hydrometeorol*. **22**, 167-183 (2021).
30. F.-C. Chang, J. M. Wallace, Meteorological conditions during heat waves and droughts in the United States Great Plains. *Mon. Weather Rev.* **115**, 1253–1269 (1987).
31. J. Cui, X. Lian, R. J. van der Ent, L. Gimeno, D. G. Miralles, Greater role of atmospheric circulation than evapotranspiration in reshaping terrestrial moisture recycling. *Sci. Bull*. **71**, 1923–1926 (2026).
32. H. Hersbach, B. Bell, P. Berrisford, G. Biavati, A. Horányi, J. Muñoz Sabater, J. Nicolas, C. Peubey, R. Radu, I. Rozum, D. Schepers, A. Simmons, C. Soci, D. Dee, J.-N. Thépaut, ERA5 monthly averaged data on single levels from 1940 to present; doi:10.24381/cds.f17050d7.
33. J. Mayer, M. Mayer, L. Haimberger, Mass-consistent atmospheric energy and moisture budget monthly data from 1979 to present derived from ERA5 reanalysis; doi:10.24381/cds.c2451f6b.
34. S. M. Vicente-Serrano, et al., A new global 0.5° gridded dataset (1901–2006) of a multiscalar drought index: Comparison with current drought index datasets based on the Palmer Drought Severity Index. *J. Hydrometeorol.* **11**, 1033–1043 (2010).
35. S. Rasp, et al., WeatherBench 2: A benchmark for the next generation of data-driven global weather models. *J. Adv. Model. Earth Syst.* **16**, e2023MS004019 (2024).
36. J. Li, T. Ding, X. Jia, X. Zhao, Analysis on the extreme heat wave over China around Yangtze River region in the summer of 2013 and its main contributing factors. *Adv. Meteorol*. **2015**, 706713 (2015).
37. V. Hari, O. Rakovec, Y. Markonis, et al., Increased future occurrences of the exceptional 2018–2019 Central European drought under global warming. *Sci. Rep.* **10**, 12207 (2020).
38. E. E. Aalbers, E. van Meijgaard, G. Lenderink, H. de Vries, B. J. J. M. van den Hurk, The 2018 west-central European drought projected in a warmer climate: how much drier can it get? *Nat. Hazards Earth Syst. Sci.* **23**, 1921–1940 (2023).
39. E. Bevacqua et al., Direct and lagged climate change effects intensified the 2022 European drought. *Nat. Geosci*. **17**, 1100–1107 (2024).
40. A. Buras, A. Rammig, C. S. Zang, Quantifying impacts of the 2018 drought on European ecosystems in comparison to 2003. *Biogeosciences* **17**, 1655-1672 (2020).
41. D. G. Miralles, P. Gentine, S. I. Seneviratne, A. J. Teuling, Land-atmospheric feedbacks during droughts and heatwaves: State of the science and current challenges. *Ann. N.Y. Acad. Sci.* **1436**, 19–35 (2019).
42. M. Zhao, G. A, Y. Liu, A. G. Konings, Evapotranspiration frequently increases during droughts. *Nat. Clim. Change* **12**, 1024–1030 (2022).

Preprint

43. A. J. Teuling, A. F. Van Loon, S. I. Seneviratne, I. Lehner, M. Aubinet, B. Heinesch, C. Bernhofer, T. Grünwald, H. Prasse, U. Spank, Evapotranspiration amplifies European summer drought. Geophys. Res. Lett. **40**, 2071-2075 (2013).
44. J. B. Basara, J. N. Maybourn, C. M. Peirano, J. E. Tate, P. J. Brown, J. D. Hoey, B. R. Smith, Drought and associated impacts in the Great Plains of the United States—A review. *Int. J. Geosci.* **4**, 72–81 (2013).
45. S. D. Schubert, M. J. Suarez, P. J. Pegion, R. D. Koster, J. T. Bacmeister, Causes of long-term drought in the U.S. Great Plains. *J. Clim.* **17**, 485–503 (2004).
46. A. Sabut, A. Mishra, D. Entekhabi, Spatiotemporal patterns of drought migration across the contiguous United States. *Water Resour. Res.* **61**, e2024WR039855 (2025).
47. R. D. Koster, et al., Impacts of local soil moisture anomalies on the atmospheric circulation and on remote surface meteorological fields during boreal summer: A comprehensive analysis over North America. *J. Clim.* **29**, 7345–7364 (2016).
48. H. Teng, G. Branstator, A. B. Tawfik, P. Callaghan, Circumglobal response to prescribed soil moisture over North America. *J. Clim.* **32**, 4525–4545 (2019).

Acknowledgments:

Funding: SK was supported by the Department of Climate, Meteorology, and Atmospheric Sciences, University of Illinois at Urbana-Champaign.

DGM was supported by the European Research Council (ERC) Consolidator grant HEAT(101088405)

Author contributions: Conceptualization: SK, FD Methodology: SK, DGM, FD Investigation: SK Visualization: SK, DM Funding acquisition: FD Project administration: FD Supervision: DGM, FD Writing – original draft: SK, FD Writing – review & editing: SK, DGM, FD

Competing interests: Authors declare that they have no competing interests.

Data, code, and materials availability: All data used in this study, including ERA5 reanalysis (32, 33), SPEI (34), and equiangular conservative 3-hourly ERA5 from WeatherBench2 (35), ERA5 drought indices (49) are available for download from the corresponding references.

Supplementary Materials

Materials and Methods

Figs. S1 to S22

Tables S1 to S2

References (*49–57*)

Preprint